
TFDNet: Time-Frequency Enhanced Decomposed Network for Long-term Time Series Forecasting

Yuxiao Luo

The Chinese University of Hong Kong, Shenzhen
Shenzhen, China
yuxiaoluo@link.cuhk.edu.cn

Ziyu Lyu

Shenzhen Institutes of Advanced Technology, Chinese Academy of Sciences
Shenzhen, China
zy.lv@siat.ac.cn

Xingyu Huang

University of Science and Technology of China
Shenzhen, China
huangxyu@mail.ustc.edu.cn

Abstract

Long-term time series forecasting is a vital task and has a wide range of real applications. Recent methods focus on capturing the underlying patterns from one single domain (e.g. the time domain or the frequency domain), and have not taken a holistic view to process long-term time series from the time-frequency domains. In this paper, we propose a **Time-Frequency Enhanced Decomposed Network (TFDNet)** to capture both the long-term underlying patterns and temporal periodicity from the time-frequency domain. In TFDNet, we devise a multi-scale time-frequency enhanced encoder backbone and develop two separate trend and seasonal time-frequency blocks to capture the distinct patterns within the decomposed trend and seasonal components in multi-resolutions. Diverse kernel learning strategies of the kernel operations in time-frequency blocks have been explored, by investigating and incorporating the potential different channel-wise correlation patterns of multivariate time series. Experimental evaluation of eight datasets from five benchmark domains demonstrated that TFDNet is superior to state-of-the-art approaches in both effectiveness and efficiency.

1 Introduction

Time series forecasting is a long-standing task, and has been widely used in various application domains, e.g. energy, weather, transportation, and economics [Rajagukguk et al. \(2020\)](#); [Angryk et al. \(2020\)](#); [Chen & Chen \(2019\)](#); [Sezer et al. \(2020\)](#). Especially, long-term time series forecasting is a challenging problem and has attracted more attention [Wu et al. \(2021\)](#); [Zhou et al. \(2022b\)](#). In recent decades, deep learning methods have made remarkable innovations in time series forecasting, from recurrent neural network (RNN) based methods [Zhang & Man \(1998\)](#); [Graves & Graves \(2012\)](#); [Chung et al. \(2014\)](#) and temporal convolution networks [Sen et al. \(2019\)](#); [Borovykh et al. \(2017\)](#); [Bai et al. \(2018\)](#) to the recent transformer-based models [Zhou et al. \(2021\)](#); [Wu et al. \(2021\)](#); [Zhou et al. \(2022b\)](#); [Nie et al. \(2022\)](#). However, the computation complexity and memory requirements of transformer-based methods make it difficult to perform long sequence modeling. Recently, simple

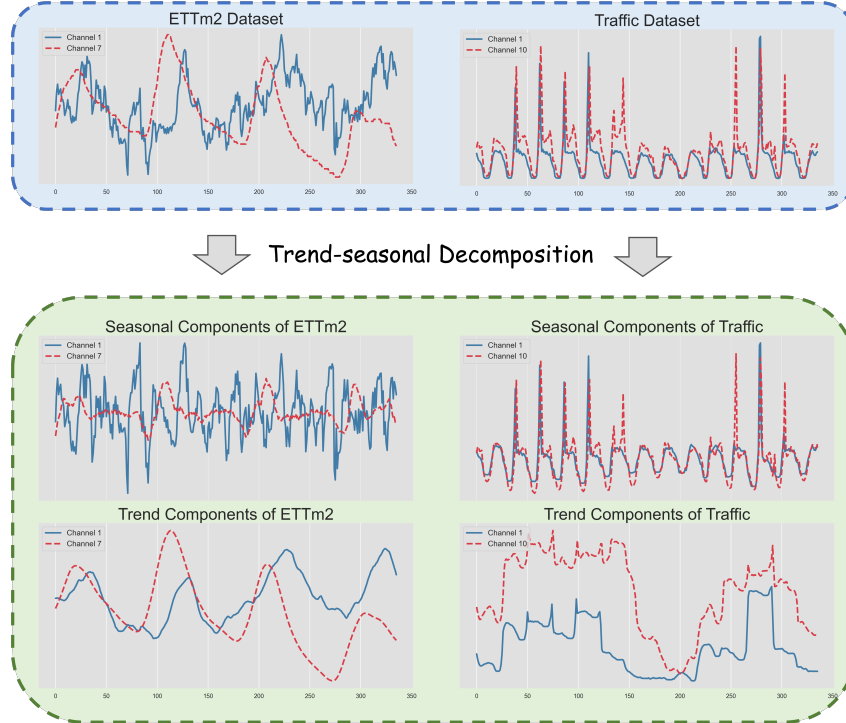


Figure 1: The top two subplots showcase the raw signals of ETTm2 and Traffic from two different channels. The lower four subplots depict the decomposed seasonal and trend components of the two datasets.

Linear models like DLiner [Zeng et al. \(2022\)](#) have been devised and achieved competitive performance with transformer-based solutions.

Despite the successful progress of diverse learning models, some issues have not been fully answered. First, the **time-frequency** information of long-term time series has not been fully studied. Most of the existing solutions focused on processing information from a single domain, e.g. the time domain or the frequency domain. For example, Autoformer [Wu et al. \(2021\)](#) and PatchTST [Nie et al. \(2022\)](#) only considered temporal periodicity and semantic learning via empowering transformer structures. FiLM [Zhou et al. \(2022a\)](#) concentrated on the frequency domain. Both time and frequency information are important for time series analysis and forecasting. The time domain includes temporal correlation and temporal periodicity, and the frequency domain can capture the global properties and the underlying change patterns of time series. Second, although some studies [Nie et al. \(2022\)](#); [Zeng et al. \(2022\)](#) have shown that adopting the channel-independence (CI) strategy can have better performance than utilizing the channel-mixing (CM), the **channel-wise correlation effects** has not been well discussed in CI strategy. Different from that the CM strategy embeds the whole channels into high-dimensional vectors to represent the entire information of all channels, while the input of CI strategy only considers the information from the single channel. In this case, channel-wise correlation is necessary to be considered when designing the model structure. In fact, the channel-wise correlations depend on the inherent characteristics of the time series data in different domains. However previous studies utilized shared parameters for all channels without considering their channel-wise correlations.

To address the above challenges, we propose a **Time-Frequency Enhanced Decomposed Network (TFDNet)** for long-term time series forecasting. **First**, we take a holistic view to process long-term time series in the time-frequency domain, by leveraging the classical signal processing method Short-time Fourier transform (STFT) [Boashash \(2015\)](#) to transform long-term time series into time-frequency matrix. **Second**, we analyze the channel-wise correlations for the whole multivariate time series in diverse domains and further investigate channel-wise correlations within the trend component and the seasonal component decomposed with the trend-seasonal decomposition block. Figure 1 illustrates various channel-wise correlations among seasonal components and trend components using the ETTm2 and Traffic datasets as an example. Regarding the trend components, there are clear relationships between the channels in these two datasets. In comparison, whereas the seasonal

components of ETTm2 are not significantly correlative, the seasonal components of Traffic exhibit a substantial association. We consider the channel-wise effects in our design of processing the trend and seasonal components. By integrating the two ideas, we devise multi-scale time-frequency enhanced encoders in **TFDNet** for the trend and seasonal components. The multi-scale windowing mechanism is devised to capture the time-frequency information in diverse resolutions. Two separate time-frequency blocks (TFBs) are respectively developed for the trend component and the seasonal component due to the distinct underlying patterns within them. In addition, we integrate the observation of different channel-wise correlation patterns into kernel operations of time-frequency blocks and introduce one individual kernel strategy and a multiple kernel sharing strategy to deal with various channel-wise correlation patterns in the seasonal component. Finally, we devise a mixture loss to enable robust forecasting, by combining the L1 loss and L2 loss. The main contributions are listed as follows:

- A Time-Frequency Enhanced Decomposed Network is proposed for robust and effective long-term time series forecasting, by taking a holistic view to process long-term time series from the time-frequency domain.
- We investigate the channel-wise correlation effects of multivariate time series forecasting, and integrate the channel-wise correlation effects into the design of separate time-frequency blocks for the trend and seasonal components.
- We conduct extensive experiments on 8 datasets in various domains, e.g. traffic, weather, electricity, etc. The experimental results demonstrated that our method is superior to state-of-the-art methods with high efficiency.

2 Related work

Time series forecasting is an important task and has a wide range of applications, e.g. traffic flow prediction, weather prediction, and energy estimation [Chen & Chen \(2019\)](#); [Rajagukguk et al. \(2020\)](#). Many methods have been proposed for time series forecasting, from the traditional statistical methods (e.g. ARIMA model [Ho & Xie \(1998\)](#)) to machine learning methods. Especially several branches of deep learning methods have been devised for long-term time series forecasting, including recurrent neural networks [Zhang & Man \(1998\)](#); [Graves & Graves \(2012\)](#); [Chung et al. \(2014\)](#), temporal convolution networks [Sen et al. \(2019\)](#); [Borovykh et al. \(2017\)](#); [Bai et al. \(2018\)](#), and the recent transformer-based solutions [Vaswani et al. \(2017\)](#); [Wu et al. \(2021\)](#); [Zhou et al. \(2021\)](#). We describe existing studies based on the utilized information domain (e.g. time domain and frequency domain) and the channel strategies of multivariate time series prediction in the following paragraphs.

Representation in time domain The temporal correlations and temporal periodicity play a vital role in time series analysis and forecasting. Transformer-based solutions have been proposed to capture the long-range dependencies within the time domain. However, transformer-based solutions have some limitations, e.g. the model complexity and large memory requirements. Informer [Zhou et al. \(2021\)](#) incorporated KL-divergence-based ProbSparse attention to reduce the model complexity. Autoformer [Wu et al. \(2021\)](#) renovated the transformer into a deep decomposition structure and designed the auto-correlation mechanism to capture temporal periodicity at the sub-series level. Non-stationary Transformer [Liu et al. \(2022\)](#) proposed series stationarization and de-stationary Attention for over-stationarization. TimesNet [Wu et al. \(2022\)](#) analyzed temporal variations from the 2D space within multiple periods.

Representation in frequency domain The underlying patterns in the frequency domain are important for time series forecasting [Sun & Boning \(2022\)](#). Therefore, several methods have leveraged frequency enhanced structure for time series forecasting. For example, FEDformer [Zhou et al. \(2022b\)](#) employed a Fourier-enhanced structure to obtain frequency domain mapping. ETSformer [Woo et al. \(2022\)](#) utilized exponential smoothing attention and frequency attention to replace the self-attention mechanism in Transformer. FiLM [Zhou et al. \(2022a\)](#) employed Legendre Polynomials projections [Voelker et al. \(2019\)](#) to approximate historical information with Fourier projection for eliminating any extraneous noise.

Channel-independence strategy Channel-independence strategy is characterized in PatchTST [Nie et al. \(2022\)](#) that each input tokens only contain information from a single channel univariate time series. PatchTST [Nie et al. \(2022\)](#) divided time series into subseries-level patches, served as input

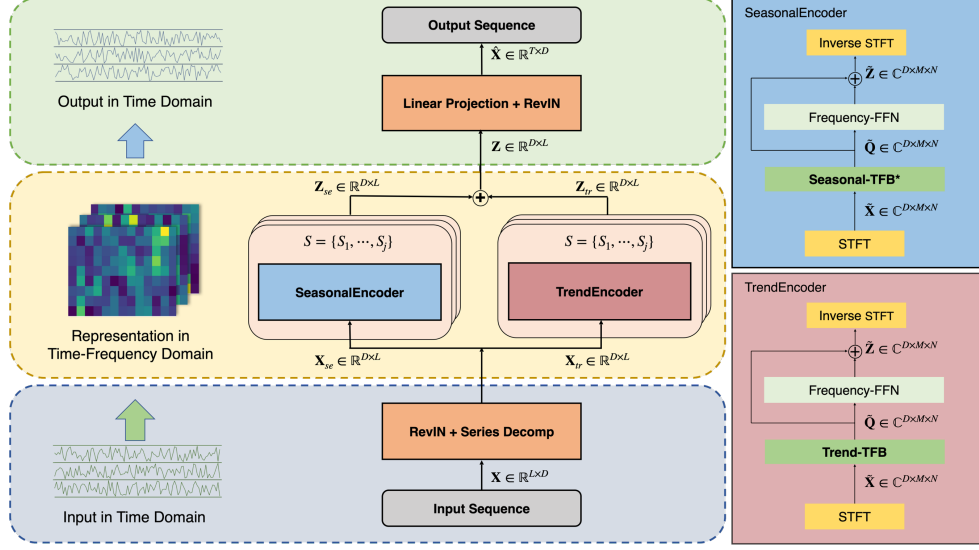


Figure 2: TFDNet architecture. The TFDNet is comprised of two branches, the seasonal branch, and the trend branch. The two branches share a common backbone with Time-Frequency Block and Frequency Feed Forward Network (Frequency-FFN) through multi-scale time-frequency enhanced encoders of S various window sizes.

tokens to Transformer. DLinear Zeng et al. (2022) challenged the effectiveness of transformer-based structures, and introduced a set of simple linear models layer for each channel. Channel-independence models can extract more historical information from a longer length of the look-back window, which increases the capacity of the model Han et al. (2023).

3 Time-frequency enhanced decomposed network

3.1 TFDNet framework

Preliminary Long-term time series forecasting is a sequence-to-sequence problem. Given the historical time series data $\mathbf{X} = [\mathbf{x}_1, \mathbf{x}_2, \dots, \mathbf{x}_L]$ with L length look-back window and each time vector \mathbf{x}_t at the t time step represents the multivariate time point with D dimension (the number of channels in the multivariate time series), the problem is to predict the future time series $\hat{\mathbf{X}} = [\hat{\mathbf{x}}_{L+1}, \dots, \hat{\mathbf{x}}_{L+T}]$, $\hat{\mathbf{X}} \in \mathbb{R}^{T \times D}$ at T future time steps ($T > 1$).

TFDNet structure The proposed TFDNet structure is shown in Figure 2 and TFDNet has three phases. In the first phase, we pre-process the input time series for further learning and the process of the first phase is defined as Equation 1. We adopt of instance normalization Kim et al. (2021); Liu et al. (2022) the historical time series \mathbf{X} to mitigate the distribution shift effects between the training and test data $\mathbf{X} = \text{RevIN}(\mathbf{X})^T$, in which each univariate time series $\mathbf{x}^{(i)}$ is normalized with zero mean and standard deviation. After instance normalization, the series decomposition block in Autoformer Wu et al. (2021) is exploited to decompose time series into the seasonal and trend components for capturing the different underlying patterns within the seasonal and trend parts.

$$\begin{aligned} \mathbf{X}_{tr} &= \text{AvgPool}(\text{Padding}(\mathbf{X})), \\ \mathbf{X}_{se} &= \mathbf{X} - \mathbf{X}_{tr}, \end{aligned} \quad (1)$$

where \mathbf{X}_{se} and \mathbf{X}_{tr} respectively denote the decomposed seasonal component and trend component. AvgPool is the moving average operation to smooth out periodic hidden variables with the padding operation to make the series length unchanged.

In the second phase, we devise multi-scale time-frequency encoders to separately capture the underlying time and frequency patterns within the seasonal and trend components. The general process of multi-scale time-frequency encoders is defined in Equation 2, and more design details are illustrated

in Section 3.2.

$$\begin{aligned}\mathbf{Z}_{se} &= \text{Linear}(\text{SeasonEncoder}(\mathbf{X}_{se}, S_1), \dots, \text{SeasonEncoder}(\mathbf{X}_{se}, S_s)), \\ \mathbf{Z}_{tr} &= \text{Linear}(\text{TrendEncoder}(\mathbf{X}_{tr}, S_1), \dots, \text{TrendEncoder}(\mathbf{X}_{tr}, S_s)),\end{aligned}\quad (2)$$

in which **TrendEncoder** and **SeasonalEncoder** are the two devised encoders, respectively represented with blue and pink boxes in Figure 2. S_1, \dots, S_s represent the utilized different sizes of window lengths. One linear layer is adopted to fuse the multi-scale seasonal representations from different scales of seasonal encoders and outputs the fused seasonal representation \mathbf{Z}_{se} . Similarly, we obtain the fused trend representation \mathbf{Z}_{tr} . Finally, we sum up the seasonal representation and the trend representation as $\mathbf{Z} = \mathbf{Z}_{se} + \mathbf{Z}_{tr}$ for the further prediction phase.

The final phase is to predict the future time series with T time steps, based on the fused encoder representation. The prediction process is defined as follows: $\hat{\mathbf{X}} = \text{RevIN}(\text{Linear}(\mathbf{Z}))$. A linear projection and instance denormalization Kim et al. (2021) are used to predict the future time series from the fused encoder representation \mathbf{Z} .

3.2 Multi-scale Time-frequency Enhanced Encoders

We adopt the multi-scale strategy to adjust the sliding window size of Short-time Fourier Transform when analyzing the time-frequency domain. As mentioned in Section 3.1, we set a different sliding window size S_e for each time-frequency encoder $_e$ and learn the time-frequency representation in multi-scale resolution. For both the seasonal encoder and the trend encoders, we have set the multi-scale sliding window sizes with $S = \{S_1, \dots, S_s\}$. With the given window size S_e , the e -th trend encoder and the e -th seasonal encoder share the same backbone structure except for the time-frequency block (TFB). For simplicity, we omit the encoder index with different scales (S) in the following paragraphs. In the following subsections, we first introduce the devised encoder structure and then demonstrate the different time-frequency blocks for the trend component (Trend-TFB) and the seasonal component (Seasonal-TFB).

3.2.1 Time-frequency enhanced encoder structure

The decomposed representation \mathbf{Z}_{tr} or \mathbf{Z}_{se} is the input into the time-frequency enhanced encoder. As the trend encoder and the seasonal encoder share the same encoder structure, we omit the subscripts (tr and se) in Section 3.2.1. The Time-frequency enhanced encoder structure has four processing parts, including Short-Time Fourier Transform (STFT), Time-frequency Block, Frequency Feed Forward Network (frequency-FFN), and Inverse Short-Time Fourier Transform (Inverse-STFT). The encoder process is defined as in Equation 3

$$\begin{aligned}\tilde{\mathbf{X}} &= \text{STFT}(\mathbf{X}), \\ \mathbf{Q} &= \text{TFB}(\tilde{\mathbf{X}}), \\ \tilde{\mathbf{Z}} &= \mathbf{Q} + \text{Frequency-FFN}(\mathbf{Q}), \\ \mathbf{Z} &= \text{STFT}^{-1}(\tilde{\mathbf{Z}}).\end{aligned}\quad (3)$$

Short-time Fourier transform: We leverage a classical method Short-time Fourier transform (STFT) to analyze the frequency content of a non-stationary signal and observe its temporal evolution Parchami et al. (2016); Griffin & Lim (1984). STFT enables the transformation of time series from the time domain to the time-frequency domain, which segments the input time series into overlapping frames and performs Discrete Fourier Transform (DFT) on each frame. The STFT process is defined as:

$$\tilde{\mathbf{X}} = \sum_{m=0}^{S-1} \text{Window}[m] \mathbf{X}[m + nl] e^{-j \frac{2\pi m \omega}{S}}, \quad (4)$$

where the window function is treated as if having 1 everywhere in the window. The output matrix from the STFT operation $\tilde{\mathbf{X}} \in \mathbb{C}^{D \times M \times N}$ denotes the outputted time-frequency matrix from $\text{STFT}(\mathbf{X})$. $M = \frac{S}{2} + 1$ denotes the size of the components of the Fourier transform according to the conjugate symmetry Dubois & Venetsanopoulos (1978). N represents the number of time frames, and $N = \frac{L}{l} + 1$ by padding the window length S . l is the stride of the moving window when performing STFT.

Time-frequency block: The Time-frequency Block (TFB) is utilized within encoders to capture the underlying patterns within the time-frequency domain. We devise the kernel operation on identical frequency bins across various time frames. For each channel (i -th channel) of the STFT output $\tilde{\mathbf{X}}^{(i)} \in \mathbb{C}^{M \times N}$, the kernel operation is generally defined as follows:

$$\mathbf{Kernel}(\tilde{\mathbf{X}}^{(i)}, \mathbf{W}) = \tilde{\mathbf{X}}_m^{(i)} \cdot \mathbf{W}_m, \quad (5)$$

in which $\mathbf{W} \in \mathbb{C}^{M \times N \times N}$ is the kernel weight matrix. $\tilde{\mathbf{X}}_m^{(i)} \in \mathbb{C}^N$ donates the m -th frequency bin and $\mathbf{W}_m \in \mathbb{C}^{N \times N}$ donates corresponding weights for the i -th channel. We devise different strategies to learn the kernel weight matrix \mathbf{W} for the trend and seasonal components, according to the inherent properties of different components. More details about the design of TFB for the trend and seasonal components are demonstrated in Section 3.2.2.

Frequency Feed Forward Network: Frequency-FFN is one fully connected layer with the activation function Tanh Fan (2000) to accumulate the time-frequency information along the **frequency** side within one time step. We combine the processed Frequency-FFN(\mathbf{Q}) and \mathbf{Q} to produce the time-frequency encoding $\tilde{\mathbf{Z}}$.

Inverse Short-time Fourier transform: \mathbf{X} can be reconstructed from $\tilde{\mathbf{X}}$, by taking the inverse Discrete Fourier Transform (DFT) of each DFT vector and overlap adding the inverted signals Parchami et al. (2016).

3.2.2 Time-frequency block

Two separate time-frequency blocks are devised for the trend component and the seasonal component, respectively Trend-TFB and Seasonal-TFB. The design of time-frequency blocks is shown in Figure 3.

Trend time-frequency block: Previous studies have found that the long-term underlying pattern of the trend component is relatively simple, compared to the seasonal component Wang et al. (2023). Therefore, we devise a simple and effective Trend-TFB to process the trend component, as shown in the top figure of Figure 3. We utilize one single shared kernel to process the trend pattern across multiple channels. We obtain $\mathbf{Q}_{tr}^{(i)} = \mathbf{Kernel}(\tilde{\mathbf{X}}^{(i)}, \mathbf{W}_{tr})$ by learning the $\mathbf{W}_{tr}^{(i)}$ for each univariate time sequence at the i -th channel with the single shared kernel. The final output of Trend-TFB is $\mathbf{Q}_{tr} \in \mathbb{C}^{D \times M \times N}$.

Seasonal time-frequency block: From the analysis studies in Figure 1, we observe that datasets in different domains have different seasonal characteristics, e.g. high seasonal correlation in Traffic, and a relatively lower correlation in ETTm2. Therefore, we design two versions to address the potential effects due to different seasonal correlation patterns among channels, respectively **seasonal-TFB with individual kernels (Seasonal-TFB-IK)** and **seasonal-TFB with multiple shared kernels (Seasonal-TFB-MK)**. The experimental results validate the essence of the specific design (individual or shared) for datasets in different domains. Different designs of the individual version (middle) and the shared version (bottom) are shown in Figure 3.

Seasonal-TFB-IK adopts the individual kernel strategy without sharing kernel weights across different channels. However, it is intractable when the channel is huge. Therefore, we leverage the low-rank approximation techniques Yuan & Yang (2009); Hyndman & Athanasopoulos (2018) to make Seasonal-TFB-IK scalable. For a large number of channels, the kernel matrix $\mathbf{W}_{ind} \in \mathbb{C}^{D \times M \times N \times N}$ is decomposed with two smaller matrices $\mathbf{W}_1 \in \mathbb{C}^{D \times I}$ and $\mathbf{W}_2 \in \mathbb{C}^{I \times M \times N \times N}$ ($I \leq D$), and $\mathbf{W}_{ind} = \mathbf{W}_1 \cdot \mathbf{W}_2$. The two smaller kernel matrices will be learned, and we have $\mathbf{Q}_{se}^{(i)} = \mathbf{Kernel}(\tilde{\mathbf{X}}_{se}^{(i)}, \mathbf{W}_{ind}^{(i)})$ for the i -th channel of the multivariate time series from Seasonal-TFB-IK.

For the data domain with high seasonal correlation, Seasonal-TFB-MK is introduced, in which we devise a multiple kernel sharing strategy and utilize one gate layer to combine the multiple kernels. Each channel is processed by multiple kernels, which can extract multiple underlying patterns across channels within the seasonal component. When having k shared kernels, we learn $\{\mathbf{W}_{multi}^1, \dots, \mathbf{W}_{multi}^k\}$ through the kernel operation for the multivariate time series. For the i -th channel time series, the output from one kernel is $\mathbf{H}_k^{(i)} = \mathbf{Kernel}(\tilde{\mathbf{X}}^{(i)}, \mathbf{W}_{multi}^k)$, and we have

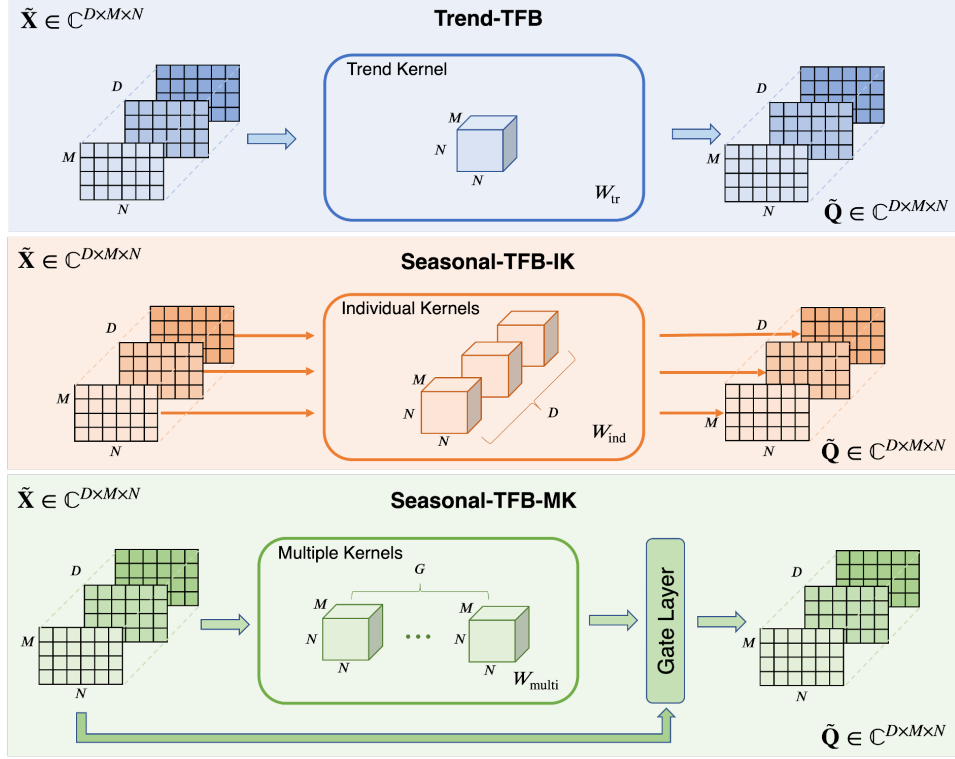


Figure 3: Workflow of Time-frequency Block. Trend-TFB is used in TrendEncoder (Top). Seasonal-TFB with individual kernels (Seasonal-TFB-IK) and seasonal-TFB with multiple shared kernels (Seasonal-TFB-MK) are used in SeasonalEncoder.

multiple kernel representations $\{\mathbf{H}_1^{(i)}, \dots, \mathbf{H}_k^{(i)}\}$. Next, the gate vector \mathbf{g} produced by $\mathbf{G}^k \in \mathbb{C}^{M \times N}$ in the gate layer is utilized to fuse the multiple kernel representations. The k -th element in the gate vector is defined as $\mathbf{g}_k = \text{Sigmod}(|\sum \mathbf{G}^k \odot \tilde{\mathbf{X}}_{se}^{(i)}|)$. Finally, $\mathbf{Q}_{se}^{(i)} = \sum_k \mathbf{g} \odot [\mathbf{H}_1^{(i)}; \mathbf{H}_2^{(i)}; \dots; \mathbf{H}_k^{(i)}]$ for the i -th channel of the multivariate time series from Seasonal-TFB-MK.

3.3 Mixture loss

The squared loss (L2) has been widely used for time series prediction [Wu et al. \(2021\)](#); [Zhou et al. \(2022b\)](#); [Nie et al. \(2022\)](#). However, the squared loss is sensitive to occasional outliers. In order to improve the robustness of the model, we combine the squared loss and the absolute loss (L1) as the mixture loss, as defined in Equation 6.

$$\mathcal{L} = \sum_{i=1}^D \alpha |\hat{\mathcal{Y}}_i - \mathcal{Y}_i| + (1 - \alpha) \|\hat{\mathcal{Y}}_i - \mathcal{Y}_i\|_2, \quad (6)$$

$$\alpha = \text{Tanh}(|\hat{\mathcal{Y}}_i - \mathcal{Y}_i|),$$

where α is to control the weights of L1 loss and L2 loss. α is based on the absolute error and uses Tanh function [Fan \(2000\)](#); [Ghosh et al. \(2017\)](#) to map the the absolute error into $(0, 1)$ as the control weights. The L1 loss plays a prominent role when the prediction error is large. The L2 loss also contributes when the error is small.

4 Experiments

Datasets We evaluate TFDNet performance on 8 widely used datasets, including Traffic, Electricity, ILLI, and 4 ETT datasets (ETTh1, ETTh2, ETTm1, ETTm2) [Wu et al. \(2021\)](#). The datasets cover four diverse application domains including energy, traffic, weather, and disease. Following previous

studies Wu et al. (2021), we split these datasets into training, validation, and test sets in chronological order, with the ratio of 6:2:2 for the ETT dataset and 7:1:2 for the remaining datasets. More details about the datasets are given in Appendix A.1.

Baselines and experimental settings We compare our proposed method with both channel-mixture (CM) models and channel-independence (CI) models. Three state-of-the-art CM models are used as baselines, including FEDformer Zhou et al. (2022b), Autoformer Wu et al. (2021), and Informer Zhou et al. (2022a). And three CI models including FiLM Zhou et al. (2022a), DLinear Zeng et al. (2022), and PatchTST Nie et al. (2022) are used as baselines. Following the experiment settings of Informer Zhou et al. (2021) and FiLM Zhou et al. (2022a), we test various lengths of the historical time series with $L \in \{96, 192, 336, 512, 720\}$. The prediction horizons T are fixed with $T \in \{24, 36, 48, 60\}$ for ILI dataset and $T \in \{96, 192, 336, 720\}$ for the remaining datasets. The commonly used evaluation metrics mean square error (MSE) and mean absolute error (MAE) are used for evaluation. All experiments are repeated 3 times. The details of the implementation setting are in Appendix A.2.

Model variants We have two versions of TFDNet, respectively TFDNet-IK and TFDNet-MK. TFDNet-IK is the model variation with the individual kernel strategy (Seasonal-TFB-IK) in Section 3.2.2 while TFDNet-MK is the version with the multiple kernel sharing strategy (Seasonal-TFB-MK). The STFT windows lengths S are set as $\{8, 16, 32\}$ for all datasets and with the strides $l = \{4, 8, 16\}$. The results from the two versions are reported in Table 1 and Table 2.

Table 1: Multivariate long-term series forecasting results on eight datasets with various prediction lengths $T \in \{96, 192, 336, 720\}$ (For ILI dataset, we set prediction length $T \in \{24, 36, 48, 60\}$). **Bold/underline** indicates the best/second.

Methods	TFDNet-IK		TFDNet-MK		PatchTST		FiLM		DLinear		FEDformer		Autoformer		Informer		
	Metric	MSE	MAE	MSE	MAE	MSE	MAE	MSE	MAE	MSE	MAE	MSE	MAE	MSE	MAE	MSE	MAE
ETTh1	96	<u>0.359</u>	<u>0.386</u>	0.356	0.383	0.373	0.402	0.377	0.401	0.375	0.396	0.376	0.416	0.449	0.455	0.916	0.741
	192	<u>0.398</u>	<u>0.412</u>	0.396	0.409	0.411	0.428	0.419	0.428	0.428	0.437	0.422	0.445	0.468	0.465	0.975	0.765
	336	<u>0.432</u>	<u>0.431</u>	0.431	0.429	<u>0.432</u>	0.445	0.466	0.466	0.448	0.449	0.452	0.463	0.506	0.494	1.099	0.819
	720	<u>0.438</u>	<u>0.453</u>	0.421	0.443	0.455	0.473	0.499	0.512	0.505	0.514	0.483	0.496	0.516	0.513	1.191	0.865
ETTh2	96	<u>0.268</u>	<u>0.329</u>	0.266	0.328	0.275	0.338	0.280	0.343	0.296	0.360	0.343	0.385	0.372	0.406	2.766	1.321
	192	<u>0.332</u>	<u>0.370</u>	0.331	0.369	0.338	0.380	0.345	0.390	0.391	0.423	0.429	0.438	0.441	0.442	6.428	2.116
	336	0.359	0.393	<u>0.361</u>	<u>0.394</u>	0.366	0.403	0.372	0.415	0.445	0.460	0.489	0.485	0.479	0.478	4.779	1.833
	720	0.381	<u>0.417</u>	0.381	0.416	0.391	0.431	0.438	0.455	0.700	0.592	0.463	0.481	0.488	0.496	3.984	1.696
ETTh1	96	0.283	0.330	0.286	0.333	0.288	0.341	0.303	0.345	0.301	0.344	0.356	0.406	0.498	0.474	0.624	0.565
	192	0.326	0.355	<u>0.327</u>	<u>0.356</u>	0.332	0.370	0.342	0.369	0.336	0.366	0.391	0.424	0.586	0.513	0.777	0.661
	336	0.359	0.377	<u>0.360</u>	<u>0.379</u>	0.362	0.392	0.371	0.387	0.371	0.387	0.441	0.453	0.657	0.543	1.087	0.799
	720	<u>0.412</u>	0.408	0.410	0.408	0.416	0.419	0.430	0.416	0.426	0.422	0.482	0.476	0.719	0.572	1.041	0.764
ETTh2	96	0.157	0.244	<u>0.158</u>	<u>0.246</u>	0.162	0.254	0.167	0.257	0.170	0.264	0.189	0.281	0.254	0.325	0.427	0.503
	192	0.213	0.282	<u>0.214</u>	<u>0.283</u>	0.217	0.293	0.219	0.293	0.233	0.311	0.257	0.324	0.280	0.336	0.812	0.700
	336	0.264	0.318	0.264	<u>0.319</u>	0.267	0.326	0.273	0.331	0.300	0.358	0.325	0.364	0.350	0.382	1.326	0.873
	720	0.345	0.371	<u>0.347</u>	<u>0.372</u>	0.353	0.382	0.356	0.387	0.422	0.439	0.429	0.424	0.437	0.429	3.986	1.532
Electricity	96	0.128	0.221	<u>0.129</u>	0.221	0.129	0.223	0.154	0.248	0.140	0.237	0.189	0.305	0.199	0.314	0.333	0.415
	192	0.145	0.237	<u>0.147</u>	<u>0.239</u>	0.149	0.243	0.167	0.260	0.154	0.250	0.205	0.320	0.215	0.325	0.344	0.427
	336	0.160	0.253	<u>0.163</u>	<u>0.256</u>	0.165	0.260	0.189	0.285	0.169	0.268	0.212	0.327	0.234	0.340	0.356	0.437
	720	0.197	0.285	<u>0.200</u>	<u>0.288</u>	<u>0.200</u>	0.292	0.250	0.341	0.204	0.300	0.245	0.352	0.289	0.380	0.386	0.450
Traffic	96	<u>0.377</u>	<u>0.256</u>	0.354	0.241	0.383	0.272	0.413	0.290	0.412	0.286	0.577	0.360	0.642	0.408	0.735	0.415
	192	<u>0.392</u>	<u>0.263</u>	0.372	0.250	<u>0.380</u>	<u>0.259</u>	0.409	0.289	0.424	0.291	0.607	0.374	0.640	0.405	0.749	0.422
	336	<u>0.406</u>	<u>0.266</u>	0.388	0.257	0.410	0.285	0.425	0.299	0.438	0.299	0.624	0.384	0.621	0.384	0.855	0.486
	720	<u>0.447</u>	<u>0.287</u>	0.428	0.279	0.454	0.313	0.525	0.373	0.467	0.317	0.625	0.381	0.709	0.435	1.094	0.619
Weather	96	0.143	0.188	0.148	0.194	<u>0.148</u>	0.200	0.194	0.234	0.175	0.235	0.221	0.304	0.271	0.341	0.382	0.437
	192	0.186	0.230	0.192	<u>0.236</u>	<u>0.191</u>	0.241	0.229	0.266	0.216	0.274	0.325	0.372	0.320	0.374	0.566	0.522
	336	0.236	0.269	0.243	<u>0.275</u>	<u>0.240</u>	0.281	0.266	0.295	0.262	0.314	0.386	0.408	0.350	0.387	0.614	0.555
	720	<u>0.314</u>	0.326	0.319	0.331	0.307	<u>0.329</u>	0.323	0.340	0.327	0.367	0.415	0.423	0.428	0.434	1.098	0.760
ILI	24	<u>1.834</u>	0.823	1.786	<u>0.829</u>	2.123	0.920	2.297	0.957	2.260	1.052	3.232	1.266	3.523	1.313	5.219	1.556
	36	<u>1.780</u>	0.834	1.764	<u>0.836</u>	1.877	0.934	2.298	0.976	2.258	1.061	3.122	1.218	3.359	1.264	5.082	1.562
	48	1.815	<u>0.861</u>	1.701	0.844	<u>1.739</u>	0.885	2.344	1.025	2.321	1.087	2.953	1.175	3.358	1.252	5.177	1.573
	60	1.756	0.861	1.910	0.936	<u>1.808</u>	<u>0.914</u>	2.151	0.952	2.478	1.130	2.858	1.159	2.892	1.150	5.280	1.584

4.1 Main results

Multivariate results From Table 1, we can see that our models outperform all baselines. In comparison with the best CM model FEDformer, TFDNet-IK with the CI strategy achieves an overall reduction of 32.3% in MSE and 22.4% in MAE, and TFDNet-MK achieves a reduction of 32.7% and 22.0%, respectively. Compared with the best CI model PatchTST, TFDNet-IK can achieve a reduction of 3.0% in MSE and 4.7% in MAE, while TFDNet-MK obtains a reduction of 3.6% and

¹The initial test data loader implemented by Autoformer discards the final incomplete batch, thereby potentially leading to an overestimation of results. All results reported in this paper are obtained after correcting this issue.

Table 2: Univariate long-term series forecasting results on ETT datasets with various prediction lengths $T \in \{96, 192, 336, 720\}$. **Bold/underline** indicates the best/second.

Methods		TFDNet-MK		PatchTST		FiLM		Dlinear		FEDformer		Autoformer		Informer	
Metric		MSE	MAE	MSE	MAE	MSE	MAE	MSE	MAE	MSE	MAE	MSE	MAE	MSE	MAE
ETT _h	96	0.054	0.176	0.054	<u>0.177</u>	0.057	0.182	0.056	0.180	0.084	0.220	0.088	0.238	0.172	0.350
	192	0.069	0.202	<u>0.071</u>	<u>0.205</u>	0.072	0.207	0.075	0.209	0.108	0.249	0.097	0.239	0.280	0.461
	336	0.077	0.221	<u>0.083</u>	<u>0.228</u>	0.084	0.230	0.092	0.238	0.123	0.278	0.104	0.260	0.256	0.428
	720	<u>0.090</u>	<u>0.237</u>	0.086	0.234	0.091	0.239	0.168	0.334	0.146	0.303	0.132	0.290	0.185	0.356
ETT ₂	96	0.126	0.274	<u>0.130</u>	<u>0.283</u>	0.128	0.273	0.132	0.280	0.129	0.271	0.152	0.303	0.221	0.381
	192	0.163	0.319	<u>0.169</u>	<u>0.328</u>	0.189	0.343	0.176	0.329	0.187	0.330	0.191	0.340	0.280	0.431
	336	0.188	0.351	<u>0.193</u>	<u>0.358</u>	0.201	0.364	0.210	0.369	0.231	0.378	0.233	0.380	0.323	0.456
	720	0.216	0.373	<u>0.221</u>	<u>0.379</u>	0.224	0.380	0.290	0.438	0.278	0.422	0.260	0.404	0.293	0.440
ETT _{m1}	96	0.026	0.121	0.026	0.121	0.029	0.128	0.028	0.125	0.034	0.143	0.050	0.174	0.103	0.264
	192	0.039	0.150	0.039	0.150	0.041	0.154	0.043	0.154	0.066	0.203	0.110	0.250	0.221	0.404
	336	0.052	0.173	<u>0.053</u>	0.173	0.053	0.174	0.062	0.183	0.071	0.210	0.085	0.236	0.219	0.387
	720	0.070	0.200	0.073	0.206	<u>0.071</u>	<u>0.205</u>	0.080	0.211	0.109	0.259	0.120	0.283	0.456	0.601
ETT _{m2}	96	0.062	0.182	<u>0.065</u>	<u>0.186</u>	0.066	0.191	0.064	0.184	0.066	0.197	0.098	0.241	0.076	0.210
	192	0.091	0.224	0.094	0.231	0.096	0.235	<u>0.092</u>	<u>0.227</u>	0.104	0.250	0.164	0.315	0.124	0.274
	336	0.117	0.260	<u>0.120</u>	<u>0.265</u>	0.123	0.269	0.122	0.265	0.155	0.303	0.178	0.325	0.163	0.314
	720	0.170	0.321	<u>0.172</u>	<u>0.322</u>	0.173	0.323	0.174	0.320	0.193	0.343	0.189	0.340	0.293	0.431

4.2%. The two versions of TFDNet demonstrate different performances on varying datasets and validate that the channel-wise correlations have important effects on the design of kernel operations (individual vs. sharing). The TFDNet-MK model has superior performance on datasets with higher channel correlations in the seasonal component, such as Traffic. Conversely, TFDNet-IK has better performance on datasets with lower channel correlations, such as ETT_{m1}, ETT_{m2}, and Weather.

Univariate results We present the univariate forecasting results on the four ETT datasets in Table 2. Similarly, TFDNet-MK has superior performance compared to all other baseline methods. Due to its single channel, TDF-IK with individual kernels is not applicable.

Table 3: Ablation of decomposition structure and time-frequency enhanced encoder. The TFNet-T utilizes only TrendEncoder without decomposition. FreqNet and TimeNet process time series in the single frequency domain and single time domain, respectively. **Bold** indicates the best.

Datasets		Traffic				Electricity				Weather				ETT _{m2}			
Prediction Length T		96	192	336	720	96	192	336	720	96	192	336	720	96	192	336	720
TFDNet-IK	MSE	0.377	0.392	0.406	0.447	0.128	0.145	0.160	0.197	0.143	0.186	0.236	0.314	0.157	0.213	0.264	0.345
	MAE	0.256	0.263	0.266	0.287	0.221	0.237	0.253	0.285	0.188	0.230	0.269	0.326	0.244	0.282	0.318	0.371
TFDNet-MK	MSE	0.354	0.372	0.388	0.428	0.129	0.147	0.163	0.200	0.148	0.192	0.243	0.319	0.158	0.214	0.264	0.347
	MAE	0.241	0.250	0.257	0.279	0.221	0.239	0.256	0.288	0.194	0.236	0.275	0.331	0.246	0.283	0.319	0.372
TFNet-T	MSE	0.372	0.391	0.405	0.442	0.130	0.146	0.163	0.200	0.147	0.192	0.243	0.318	0.159	0.214	0.266	0.348
	MAE	0.252	0.260	0.266	0.287	0.223	0.238	0.255	0.288	0.193	0.235	0.275	0.329	0.246	0.284	0.319	0.373
FreqNet	MSE	0.385	0.396	0.409	0.446	0.136	0.149	0.165	0.204	0.165	0.207	0.256	0.322	0.158	0.214	0.265	0.351
	MAE	0.260	0.264	0.270	0.290	0.229	0.240	0.257	0.290	0.212	0.249	0.286	0.334	0.246	0.287	0.320	0.376
TimeNet	MSE	0.393	0.403	0.415	0.453	0.136	0.148	0.164	0.203	0.169	0.212	0.258	0.326	0.159	0.215	0.268	0.353
	MAE	0.262	0.265	0.271	0.291	0.230	0.240	0.257	0.289	0.215	0.252	0.288	0.338	0.247	0.286	0.322	0.376

4.2 Ablation studies

To inspect the effects of some main components, we perform ablation studies by removing the decomposition structure and investigating different variants of time-frequency enhanced encoders (FreqNet and TimeNet). The ablation results are shown in Table 3.

Ablation of decomposition structure TFNet-T only keeps TrendEncoder with Trend-TFB to process the original data, removing the decomposition process. We can see that the performance of TFNet-T drops, which indicates the effects of Seasonal-TFB with individual kernels or multiple kernels in the decomposition structure.

Ablation of time-frequency enhanced encoder We investigate the effects of different operations in the time-frequency enhanced encoder. We have two variants FreqNet and TimeNet. FreqNet only utilizes the information from the frequency domain through Frequency-FFN. TimeNet replaces the encoder with two linear layers to learn the representation from the time domain in the seasonal and trend branches. We can see that the performance of the two variants remarkably drops. It verifies the effects of the time-frequency enhanced operations in the time-frequency enhanced encoder.

Table 4: Memory usages and running time per epoch of PatchTST, FiLM, and TFDNet. The "-" indicates the out-of-memory. **Bold** indicates the best.

Methods	Memory Usage (MB)					Runing Time Per Epoch (s)				
	192	336	720	1440	2880	192	336	720	1440	2880
PatchTST	3708	5292	13892	43866	-	200	305	635	1879	-
FiLM	10300	16834	34338	-	-	715	1159	2302	-	-
TFDNet-IK	712	866	2046	6272	22722	177	190	222	405	949
TFDNet-MK	1106	1196	2524	4676	10192	188	191	249	416	818

4.3 Model efficiency

Running efficiency plays a crucial role in time series forecasting. We utilize the Electricity dataset as an example to investigate the model efficiency (speed and memory usage). In the Electricity dataset, the channel number is 321 and the batch size is set as 8. The prediction horizon T is fixed at 720 and we increase the look-back window L from 192 to 2880. All results are running on a single NVIDIA RTX A6000 48GB GPU. Compared with other channel-independence models FiLM and PatchTST, our proposed TFDNets achieve higher efficiency by reducing the model complexity in terms of both memory usage and training speed per epoch. The computational complexity of the TFB kernel operation is $\mathcal{O}(MN^2)$ ($N \ll L, M \ll L$). When the input length scales up, we reduce memory usage and running time with up to $9.4\times$ and $4.63\times$, respectively. When L is very large, e.g. 1440 or 2880, the compared models cannot run due to out of max memory usage of a single GPU while our method is scaleable with the large input length.

5 Conclusion and limitation

We take a holistic view to process long-term time series from the time-frequency domain and propose TFDNet by leveraging Short-time Fourier transform (STFT) to transform long-term time series into time-frequency matrixes. And multi-scale time-frequency enhanced encoders are devised, in which two separate time-frequency blocks (TFBs) are respectively developed for the trend component and the seasonal component to extract the distinct underlying patterns within the two components. The observation of different channel-wise correlation patterns is integrated into kernel operations of time-frequency blocks and two kernel learning strategies (individual vs. sharing) are explored to deal with various channel-wise correlation patterns in the seasonal component. Experiment results validate the effectiveness and efficiency of TFDNet. Although the two versions of TFDNet have achieved superior performances, the model selection is mainly based on the channel-wise correlation effects. Further investigations and theoretical studies should be considered.

References

- Angryk, R. A., Martens, P. C., Aydin, B., Kempton, D., Mahajan, S. S., Basodi, S., Ahmadzadeh, A., Cai, X., Filali Boubrahimi, S., Hamdi, S. M., et al. Multivariate time series dataset for space weather data analytics. *Scientific data*, 7(1):227, 2020.
- Bai, S., Kolter, J. Z., and Koltun, V. An empirical evaluation of generic convolutional and recurrent networks for sequence modeling. *arXiv preprint arXiv:1803.01271*, 2018.
- Boashash, B. *Time-frequency signal analysis and processing: a comprehensive reference*. Academic press, 2015.
- Borovykh, A., Bohte, S., and Oosterlee, C. W. Conditional time series forecasting with convolutional neural networks. *arXiv preprint arXiv:1703.04691*, 2017.
- Chen, X. and Chen, R. A review on traffic prediction methods for intelligent transportation system in smart cities. In *2019 12th International Congress on Image and Signal Processing, BioMedical Engineering and Informatics (CISP-BMEI)*, pp. 1–5. IEEE, 2019.
- Chung, J., Gulcehre, C., Cho, K., and Bengio, Y. Empirical evaluation of gated recurrent neural networks on sequence modeling. *arXiv preprint arXiv:1412.3555*, 2014.
- Dubois, E. and Venetsanopoulos, A. Convolution using a conjugate symmetry property for the generalized discrete fourier transform. *IEEE Transactions on Acoustics, Speech, and Signal Processing*, 26(2):165–170, 1978.
- Fan, E. Extended tanh-function method and its applications to nonlinear equations. *Physics Letters A*, 277(4-5):212–218, 2000.
- Ghosh, A., Kumar, H., and Sastry, P. S. Robust loss functions under label noise for deep neural networks. In *Proceedings of the AAAI conference on artificial intelligence*, volume 31, 2017.
- Graves, A. and Graves, A. Long short-term memory. *Supervised sequence labelling with recurrent neural networks*, pp. 37–45, 2012.
- Griffin, D. and Lim, J. Signal estimation from modified short-time fourier transform. *IEEE Transactions on acoustics, speech, and signal processing*, 32(2):236–243, 1984.
- Han, L., Ye, H.-J., and Zhan, D.-C. The capacity and robustness trade-off: Revisiting the channel independent strategy for multivariate time series forecasting. *arXiv preprint arXiv:2304.05206*, 2023.
- Ho, S. L. and Xie, M. The use of arima models for reliability forecasting and analysis. *Computers & industrial engineering*, 35(1-2):213–216, 1998.
- Hyndman, R. J. and Athanasopoulos, G. *Forecasting: principles and practice*. OTexts, 2018.
- Kim, T., Kim, J., Tae, Y., Park, C., Choi, J.-H., and Choo, J. Reversible instance normalization for accurate time-series forecasting against distribution shift. In *International Conference on Learning Representations*, 2021.
- Kingma, D. P. and Ba, J. Adam: A method for stochastic optimization. *arXiv preprint arXiv:1412.6980*, 2014.
- Liu, Y., Wu, H., Wang, J., and Long, M. Non-stationary transformers: Rethinking the stationarity in time series forecasting. *arXiv preprint arXiv:2205.14415*, 2022.
- Nie, Y., Nguyen, N. H., Sinthong, P., and Kalagnanam, J. A time series is worth 64 words: Long-term forecasting with transformers. *arXiv preprint arXiv:2211.14730*, 2022.
- Parchami, M., Zhu, W.-P., Champagne, B., and Plourde, E. Recent developments in speech enhancement in the short-time fourier transform domain. *IEEE Circuits and Systems Magazine*, 16(3): 45–77, 2016.

- Paszke, A., Gross, S., Massa, F., Lerer, A., Bradbury, J., Chanan, G., Killeen, T., Lin, Z., Gimelshein, N., Antiga, L., et al. Pytorch: An imperative style, high-performance deep learning library. *Advances in neural information processing systems*, 32, 2019.
- Rajagukguk, R. A., Ramadhan, R. A., and Lee, H.-J. A review on deep learning models for forecasting time series data of solar irradiance and photovoltaic power. *Energies*, 13(24):6623, 2020.
- Sen, R., Yu, H.-F., and Dhillon, I. S. Think globally, act locally: A deep neural network approach to high-dimensional time series forecasting. *Advances in neural information processing systems*, 32, 2019.
- Sezer, O. B., Gudelek, M. U., and Ozbayoglu, A. M. Financial time series forecasting with deep learning: A systematic literature review: 2005–2019. *Applied soft computing*, 90:106181, 2020.
- Sun, F.-K. and Boning, D. S. Fredo: frequency domain-based long-term time series forecasting. *arXiv preprint arXiv:2205.12301*, 2022.
- Vaswani, A., Shazeer, N., Parmar, N., Uszkoreit, J., Jones, L., Gomez, A. N., Kaiser, Ł., and Polosukhin, I. Attention is all you need. *Advances in neural information processing systems*, 30, 2017.
- Voelker, A., Kajić, I., and Eliasmith, C. Legendre memory units: Continuous-time representation in recurrent neural networks. *Advances in neural information processing systems*, 32, 2019.
- Wang, H., Peng, J., Huang, F., Wang, J., Chen, J., and Xiao, Y. Micn: Multi-scale local and global context modeling for long-term series forecasting. In *The Eleventh International Conference on Learning Representations*, 2023.
- Woo, G., Liu, C., Sahoo, D., Kumar, A., and Hoi, S. Etsformer: Exponential smoothing transformers for time-series forecasting. *arXiv preprint arXiv:2202.01381*, 2022.
- Wu, H., Xu, J., Wang, J., and Long, M. Autoformer: Decomposition transformers with auto-correlation for long-term series forecasting. *Advances in Neural Information Processing Systems*, 34:22419–22430, 2021.
- Wu, H., Hu, T., Liu, Y., Zhou, H., Wang, J., and Long, M. Timesnet: Temporal 2d-variation modeling for general time series analysis. *arXiv preprint arXiv:2210.02186*, 2022.
- Yuan, X. and Yang, J. Sparse and low-rank matrix decomposition via alternating direction methods. *preprint*, 12(2), 2009.
- Zeng, A., Chen, M., Zhang, L., and Xu, Q. Are transformers effective for time series forecasting? *arXiv preprint arXiv:2205.13504*, 2022.
- Zhang, J. and Man, K.-F. Time series prediction using rnn in multi-dimension embedding phase space. In *SMC'98 Conference Proceedings. 1998 IEEE International Conference on Systems, Man, and Cybernetics (Cat. No. 98CH36218)*, volume 2, pp. 1868–1873. IEEE, 1998.
- Zhou, H., Zhang, S., Peng, J., Zhang, S., Li, J., Xiong, H., and Zhang, W. Informer: Beyond efficient transformer for long sequence time-series forecasting. In *Proceedings of the AAAI conference on artificial intelligence*, volume 35, pp. 11106–11115, 2021.
- Zhou, T., Ma, Z., Wen, Q., Sun, L., Yao, T., Yin, W., Jin, R., et al. Film: Frequency improved legendre memory model for long-term time series forecasting. *Advances in Neural Information Processing Systems*, 35:12677–12690, 2022a.
- Zhou, T., Ma, Z., Wen, Q., Wang, X., Sun, L., and Jin, R. Fedformer: Frequency enhanced decomposed transformer for long-term series forecasting. In *International Conference on Machine Learning*, pp. 27268–27286. PMLR, 2022b.

A Datasets and Implementation Details

A.1 Dataset Details

This subsection provides a summary of the datasets utilized in this paper: 1) ETT¹ (Electricity Transformer Temperature) dataset contains two electric transformers, ETT1 and ETT2, collected from two separate counties. Each of them has two versions of sampling resolutions (15min & 1h). Thus, there are four ETT datasets: ETTm1, ETTm2, ETTh1, and ETTh2. 2) Electricity² dataset contains the hourly electricity consumption for 321 customers. 3) Traffic³ dataset contains the freeway occupation rate from 862 different sensors in California, USA. 4) Weather⁴ dataset contains 21 meteorological indicators in Germany, such as humidity and air temperature. 5) Illness⁵ dataset contains the number of influenza-like illness patients weekly in the United States. Table 5 summarizes the features of the five benchmark datasets.

Table 5: Details of benchmark datasets.

Dataset	ETTm1	ETTm2	ETTh1	ETTh2	Electricity	Weather	Traffic	ILI
Length	69680	69680	17420	17420	26304	52696	17544	966
Feature	7	7	7	7	321	21	862	7
Frequency	15 min	15 min	1 h	1 h	1 h	10 min	1 h	7 days

The Exchange-rate⁶ dataset is used as the benchmark dataset, similar to PatchTST because the financial datasets exhibit distinct characteristics in comparison to time series datasets in other domains, such as their level of predictability Nie et al. (2022).

A.2 Implementation Details

TFDNet-IK employs Seasonal-TFB-IK with individual parameters across channels in SeasonalEncoder, which uses the individual factor $I = D$ for datasets with few channels (ETT, Weather, and ILI) and $I = 64$ for datasets with large channels (Traffic and Electricity). TFDNet-MK utilizes Seasonal-TFB-MK with shared parameters across channels in Seasonal Encoder, which use the number of kernels $k = 4$ for datasets with few channels (ETT, Weather, and ILI) and $k = 16$ for datasets with large channels (Traffic and Electricity) considering the balance between performance and efficiency.

Our model is trained with the proposed Mixture loss in section 3.3, using the Adam Kingma & Ba (2014) optimizer with an initial learning rate from $5e^{-5}$ to $5e^{-3}$. We also tune the learning rate with the cosine decay schedule. The batch size is set to 128 for the small dataset, eg. ETT, and 32 for the large dataset, eg. Traffic due to the limitation of GPU memory usage. The default training process is 50 epochs (100 epochs for Electricity and Traffic) within 10 epochs early stopping. We save the best model with the lowest loss on the validation as the final testing. All experiments are repeated 3 times, implemented in PyTorch Paszke et al. (2019) and conducted on a single NVIDIA RTX A6000 48GB GPUs which is sufficient for all our experiments.

B Experiment Error Bars

We train all models 3 times and calculate the error bars for TFDNet and another two SOTA models (PatchTST and FiLM) for evaluating the robustness of models. The results are shown in Table 6. We can see our proposed TFDNet-IK and TFDNet-MK are able to outperform the other models with lower standard deviation.

¹<https://github.com/zhouhaoyi/ETDataset>

²<https://archive.ics.uci.edu/ml/datasets/ElectricityLoadDiagrams20112014>

³<http://pems.dot.ca.gov>

⁴<https://www.bgc-jena.mpg.de/wetter/>

⁵<https://gis.cdc.gov/grasp/fluview/fluportaldashboard.html>

⁶<https://github.com/laiquokun/multivariate-time-series-data>

Table 6: Multivariate long-term series forecasting results with error bars (Mean and STD). All experiments are repeated 3 times. **Bold** indicates the best.

Methods	TFDNet-IK		TFDNet-MK		PatchTST		FiLM		
	Metric	MSE	MAE	MSE	MAE	MSE	MAE	MSE	MAE
ETTh1	96	0.3590±0.0014	0.3861±0.0003	0.3560±0.0003	0.3833±0.0002	0.3732±0.0009	0.4023±0.0008	0.3772±0.0021	0.4012±0.0024
	192	0.3976±0.0015	0.4120±0.0010	0.3957±0.0005	0.4090±0.0008	0.4111±0.0014	0.4277±0.0015	0.4193±0.0020	0.4283±0.0022
	336	0.4319±0.0011	0.4310±0.0007	0.4308±0.0011	0.4290±0.0013	0.4323±0.0059	0.4455±0.0048	0.4659±0.0040	0.4663±0.0037
	720	0.4380±0.0016	0.4530±0.0016	0.4208±0.0034	0.4433±0.0033	0.4552±0.0049	0.4728±0.0038	0.4993±0.0055	0.5120±0.0039
ETTh2	96	0.2675±0.0012	0.3291±0.0008	0.2658±0.0002	0.3281±0.0003	0.2745±0.0011	0.3379±0.0006	0.28±0.0005	0.3429±0.0003
	192	0.3316±0.0010	0.3695±0.0006	0.3306±0.0016	0.3687±0.0009	0.3383±0.0020	0.3798±0.0015	0.3452±0.0020	0.3895±0.0011
	336	0.3590±0.0012	0.3935±0.0006	0.3610±0.0013	0.3944±0.0008	0.3655±0.0011	0.4032±0.0005	0.3716±0.0022	0.4147±0.0012
	720	0.3814±0.0014	0.4172±0.0012	0.3809±0.0017	0.4163±0.0019	0.3914±0.0021	0.4310±0.0016	0.4380±0.0039	0.4548±0.0038
ETTh1	96	0.2830±0.0010	0.3298±0.0006	0.2859±0.0005	0.3325±0.0004	0.2882±0.0006	0.3413±0.0010	0.3028±0.0004	0.3448±0.0004
	192	0.3264±0.0007	0.3554±0.0005	0.3274±0.0001	0.3564±0.0004	0.3320±0.0009	0.3699±0.0007	0.3418±0.0014	0.3695±0.0006
	336	0.3590±0.0009	0.3767±0.0005	0.3595±0.0022	0.3786±0.0018	0.3617±0.0018	0.3922±0.0002	0.3712±0.0008	0.3871±0.0004
	720	0.4121±0.0013	0.4079±0.0005	0.4101±0.0001	0.4082±0.0003	0.4160±0.0002	0.4186±0.0003	0.4297±0.0009	0.4162±0.0007
ETTh2	96	0.1569±0.0006	0.2439±0.0007	0.1584±0.0002	0.2462±0.0009	0.1624±0.0008	0.2543±0.0004	0.1674±0.0009	0.2573±0.0004
	192	0.2129±0.0000	0.2821±0.0001	0.2136±0.0002	0.2834±0.0002	0.2168±0.0009	0.2932±0.0006	0.2193±0.0002	0.2934±0.0003
	336	0.2636±0.0004	0.3176±0.0003	0.2638±0.0005	0.3186±0.0002	0.2670±0.0005	0.3263±0.0005	0.2727±0.0006	0.3305±0.0007
	720	0.3445±0.0011	0.3706±0.0003	0.3468±0.0007	0.3723±0.0005	0.3526±0.0029	0.3819±0.0027	0.3563±0.0007	0.3875±0.0009
Electricity	96	0.1277±0.0001	0.2210±0.0001	0.1289±0.0003	0.2215±0.0004	0.1290±0.0005	0.2226±0.0005	0.1544±0.0000	0.2482±0.0002
	192	0.1453±0.0002	0.2372±0.0001	0.1466±0.0006	0.2386±0.0007	0.1489±0.0006	0.2427±0.0014	0.1669±0.0002	0.2599±0.0003
	336	0.1604±0.0004	0.2533±0.0004	0.1630±0.0004	0.2556±0.0003	0.1646±0.0010	0.2599±0.0012	0.1895±0.0001	0.2847±0.0003
	720	0.1965±0.0010	0.2853±0.0006	0.2001±0.0005	0.2878±0.0004	0.2003±0.0027	0.2919±0.0020	0.2501±0.0003	0.3411±0.0002
Traffic	96	0.3767±0.0015	0.2557±0.0004	0.3542±0.0007	0.2412±0.0008	0.3834±0.0182	0.2715±0.0174	0.4133±0.0012	0.2897±0.0001
	192	0.3916±0.0001	0.2625±0.0001	0.3720±0.0005	0.2496±0.0003	0.3798±0.0011	0.2587±0.0007	0.4087±0.0001	0.2888±0.0002
	336	0.4063±0.0008	0.2657±0.0007	0.3880±0.0008	0.2567±0.0008	0.4099±0.0129	0.2847±0.0147	0.4255±0.0006	0.2993±0.0008
	720	0.4474±0.0020	0.2872±0.0008	0.4285±0.0016	0.2786±0.0019	0.4538±0.0018	0.3129±0.0014	0.5253±0.0009	0.3729±0.0002
Weather	96	0.1427±0.0002	0.1883±0.0001	0.1479±0.0004	0.1941±0.0000	0.1481±0.0029	0.1997±0.0035	0.1938±0.0009	0.2344±0.0005
	192	0.1859±0.0003	0.2296±0.0007	0.1923±0.0002	0.2358±0.0005	0.1913±0.0025	0.2410±0.0017	0.2293±0.0003	0.2656±0.0002
	336	0.2356±0.0005	0.2693±0.0004	0.2426±0.0004	0.2754±0.0002	0.2403±0.0010	0.2809±0.0018	0.2661±0.0003	0.2950±0.0004
	720	0.3138±0.0019	0.3257±0.0016	0.3188±0.0012	0.3310±0.0006	0.3068±0.0012	0.3288±0.0015	0.3231±0.0007	0.3398±0.0008
ILI	24	1.8344±0.0036	0.8229±0.0106	1.7857±0.0136	0.8289±0.0038	2.1226±0.1164	0.9201±0.0364	2.2966±0.0550	0.9567±0.0242
	36	1.7797±0.0111	0.8340±0.0069	1.7640±0.0550	0.8361±0.0187	1.8773±0.1362	0.9341±0.0619	2.2983±0.0507	0.9765±0.0319
	48	1.8154±0.0496	0.8614±0.0231	1.7011±0.1103	0.8445±0.0375	1.7393±0.0941	0.8852±0.0382	2.3440±0.0808	1.0248±0.0166
	60	1.7563±0.0528	0.8613±0.0187	1.9102±0.1089	0.9365±0.0389	1.8076±0.0763	0.9141±0.0220	2.1510±0.0124	0.9519±0.0083

C Hyper-parameter Sensitivity

Influence of Individual factor For Seasonal-TFB-IK in TFDNet-IK, we study the sensitivity of various individual factors I on four datasets (Traffic, Electricity, Weather, and ETTh2) with a fixed prediction length $T = 96$. The individual factor is set as $I = \{4, 16, 32, 64\}$. As shown in Table 7, different individual factors have no significant effects on the results, which verifies the model robustness with the individual factor I .

Table 7: TDFNet-IK performance under different choices of individual factor I in the Seasonal-TFB-IK.

Individual Factor I	4		16		32		64	
	MSE	MAE	MSE	MAE	MSE	MAE	MSE	MAE
Electricity	0.128	0.221	0.127	0.220	0.127	0.220	0.128	0.221
Traffic	0.374	0.252	0.370	0.250	0.374	0.250	0.377	0.256
Weather	0.143	0.189	0.142	0.188	0.143	0.188	0.143	0.188
ETTh2	0.157	0.244	0.157	0.243	0.157	0.244	0.157	0.244

Influence of Kernel number For Seasonal-TFB-MK in TFDNet-MK, we explore the effects of different kernel numbers on four datasets (Traffic, Electricity, Weather, and ETTh2). To trade-off performance and efficiency, we set $k = \{1, 4, 8, 16\}$. As shown in Table 8, models with multiple kernels have better performance than a single kernel. Especially for datasets with a large number of channels like Traffic, more kernels can improve the performance.

D Additional Experiments

D.1 Loss Effect Analysis

L2 loss function is commonly utilized in many time series forecasting models to measure the dissimilarity between the predicted and actual values Wu et al. (2021); Zhou et al. (2022b); Nie et al.

Table 8: TDFNet-MK performance under different choices of kernel number k in the Seasonal-TFB-MK.

Kernel number k	1		4		8		16	
Metric	MSE	MAE	MSE	MAE	MSE	MAE	MSE	MAE
Electricity	0.130	0.223	0.129	0.222	0.129	0.222	0.129	0.221
Traffic	0.368	0.250	0.362	0.248	0.361	0.247	0.354	0.241
Weather	0.151	0.204	0.148	0.194	0.150	0.204	0.153	0.206
ETTM2	0.158	0.245	0.158	0.246	0.158	0.245	0.160	0.247

Table 9: Multivariate long-term series forecasting results from training with two different loss functions. ML represents our proposed Mixture loss function and L2 represents L2 loss function. **Bold** indicates the best.

Methods		TFDNet-IK(ML)		TFDNet-IK(L2)		TFDNet-MK(ML)		TFDNet-MK(L2)	
Metric		MSE	MAE	MSE	MAE	MSE	MAE	MSE	MAE
ETTh1	96	0.359	0.386	0.364	0.394	0.356	0.383	0.361	0.390
	192	0.398	0.412	0.395	0.416	0.396	0.409	0.393	0.411
	336	0.432	0.431	0.424	0.437	0.431	0.429	0.428	0.434
	720	0.438	0.453	0.455	0.475	0.421	0.443	0.439	0.464
ETTh2	96	0.268	0.329	0.268	0.332	0.266	0.328	0.265	0.331
	192	0.332	0.370	0.329	0.369	0.331	0.369	0.329	0.369
	336	0.359	0.393	0.354	0.393	0.361	0.394	0.353	0.393
	720	0.381	0.417	0.387	0.422	0.381	0.416	0.381	0.422
ETTh1	96	0.283	0.330	0.283	0.339	0.286	0.333	0.288	0.343
	192	0.326	0.355	0.323	0.365	0.327	0.356	0.326	0.365
	336	0.359	0.377	0.356	0.385	0.360	0.379	0.359	0.387
	720	0.412	0.408	0.407	0.414	0.410	0.408	0.409	0.414
ETTh2	96	0.157	0.244	0.159	0.249	0.158	0.246	0.161	0.253
	192	0.213	0.282	0.212	0.287	0.214	0.283	0.215	0.290
	336	0.264	0.318	0.263	0.322	0.264	0.319	0.265	0.324
	720	0.345	0.371	0.346	0.374	0.347	0.372	0.347	0.376
Electricity	96	0.128	0.221	0.129	0.226	0.129	0.221	0.129	0.225
	192	0.145	0.237	0.145	0.240	0.147	0.239	0.147	0.242
	336	0.160	0.253	0.161	0.257	0.163	0.256	0.164	0.260
	720	0.197	0.285	0.194	0.290	0.200	0.288	0.200	0.292
Traffic	96	0.377	0.256	0.379	0.275	0.354	0.241	0.361	0.261
	192	0.392	0.263	0.395	0.281	0.372	0.250	0.379	0.269
	336	0.406	0.266	0.409	0.286	0.388	0.257	0.393	0.275
	720	0.447	0.287	0.444	0.306	0.428	0.279	0.433	0.295
Weather	96	0.143	0.188	0.146	0.200	0.148	0.194	0.153	0.208
	192	0.186	0.230	0.192	0.241	0.192	0.236	0.194	0.246
	336	0.236	0.269	0.238	0.282	0.243	0.275	0.246	0.287
	720	0.314	0.326	0.313	0.334	0.319	0.331	0.320	0.339
ILL	24	1.834	0.823	1.981	0.891	1.786	0.829	1.824	0.860
	36	1.780	0.834	2.230	1.037	1.764	0.836	1.784	0.860
	48	1.815	0.861	2.188	1.028	1.701	0.844	1.938	0.956
	60	1.756	0.861	2.045	0.983	1.910	0.936	2.176	1.037

(2022). We conduct experiments to study the effects of different loss functions. Our models are retrained by L2 loss function with the same settings and the results are in Table 9. However, L2 loss is sensitive to outliers which makes it is easier to be affected by noises. Noise is abundant in real-time series, in this case, sensitivity to noise reduces the robustness of the model.

As shown in Table 9, our proposed Mixture loss can improve the prediction accuracy with lower MSE in most cases. And in all cases, Mixture loss function is able to make models more robust with lower MAE, compared with L2 loss.

D.2 Multi-scale Strategy Effect Analysis

We employ the multi-scale strategy to adjust the sliding window size of STFT to capture the time-frequency information in diverse resolutions. To analyze the effects of the multi-scale strategy with multiple STFT window lengths, we evaluate TFDNet with a single fixed window size on four datasets (Traffic, Electricity, Weather, ETTm2). As shown in Table 10, the two versions of TFDNet with multi-scale strategy have better performance on Traffic and Electricity datasets. However, it does not work well on ETTm2 dataset.

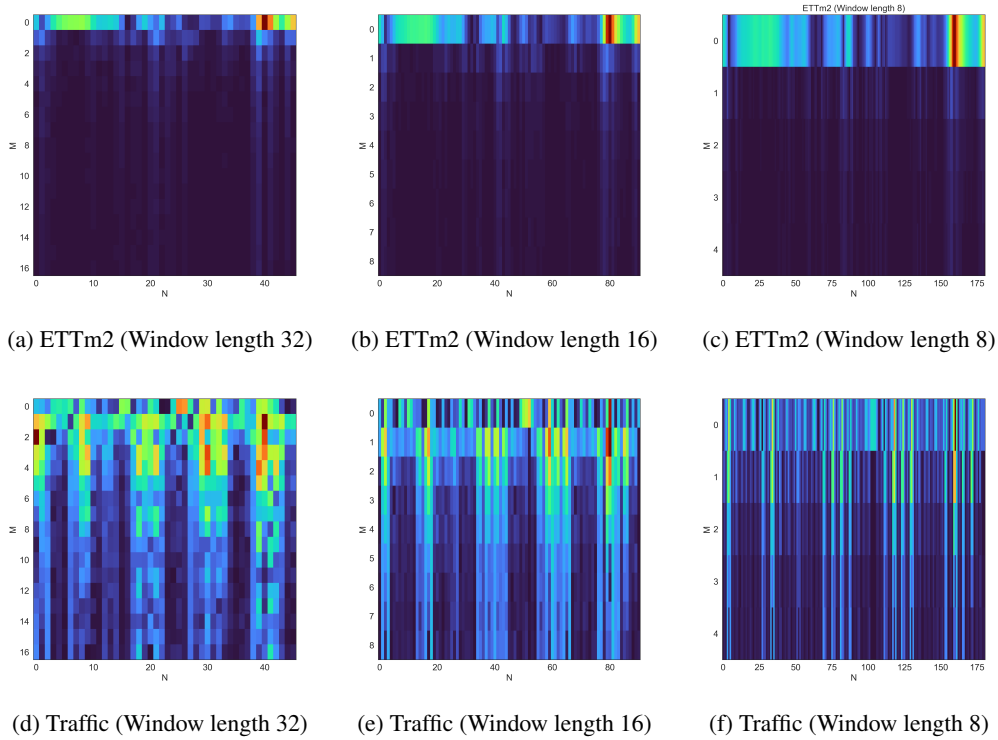


Figure 4: Time-frequency maps of ETTm2 and Traffic datasets with STFT window length $\{8, 16, 32\}$.

This phenomenon can be explained by their time-frequency maps. As shown in Figure 4, the historical information of ETTm2 is mainly from the lowest frequency component in multi-resolutions, with little information from the higher frequency components. The historical information of Traffic dataset is distributed over different frequency components by comparison, and the multi-scale windows are able to capture the time-frequency information in diverse resolutions.

Table 10: The performance of TFDNet using the multi-scale strategy and the single strategy. Multi-scale strategy sets the STFT windows lengths S as $\{8, 16, 32\}$, and single strategy sets S as 16.

Datasets		Traffic				Electricity				Weather				ETTM2			
Prediction Length T		96	192	336	720	96	192	336	720	96	192	336	720	96	192	336	720
TFDNet-IK	MSE	0.377	0.392	0.406	0.447	0.128	0.145	0.160	0.197	0.143	0.186	0.236	0.314	0.157	0.213	0.264	0.345
	MAE	0.256	0.263	0.266	0.287	0.221	0.237	0.253	0.285	0.188	0.230	0.269	0.326	0.244	0.282	0.318	0.371
TFDNet-IK (Single)	MSE	0.377	0.393	0.408	0.449	0.128	0.146	0.162	0.200	0.144	0.187	0.237	0.313	0.157	0.211	0.264	0.346
	MAE	0.256	0.264	0.270	0.290	0.221	0.237	0.254	0.287	0.189	0.230	0.270	0.325	0.244	0.282	0.318	0.371
TFDNet-MK	MSE	0.354	0.372	0.388	0.428	0.129	0.147	0.163	0.200	0.148	0.192	0.243	0.319	0.158	0.213	0.264	0.346
	MAE	0.241	0.250	0.257	0.279	0.221	0.239	0.256	0.288	0.194	0.236	0.275	0.331	0.246	0.284	0.319	0.372
TFDNet-MK (Single)	MSE	0.361	0.379	0.394	0.433	0.130	0.147	0.164	0.202	0.148	0.193	0.243	0.317	0.158	0.214	0.264	0.347
	MAE	0.246	0.254	0.261	0.281	0.222	0.239	0.256	0.289	0.194	0.236	0.276	0.330	0.246	0.283	0.319	0.372

D.3 Investigation of Trend-TFB

Trend-TFB has a simpler structure and higher efficiency than Seasonal-TFB. To validate whether Trend-TFB is adequate to capture the trend information, we analyze the effects of the complex version of Trend-TFB with multiple kernels (similar to the multiple kernel strategy in Seasonal-TFB). Therefore, we have two additional versions, by changing the simple Trend-TFB with Trend-TFB with multiple kernels, respectively TFDNet-MK-IK and TFDNet-2MK for the subversions of Seasonal-TFB. TFDNet-MK-IK denotes to use Trend-TFB with multiple kernels and Seasonal-TFB-IK while TFDNet-2MK denotes to use Trend-TFB with multiple kernels and Seasonal-TFB-MK. The analysis results are shown in Table 11. We can see that TFDNet-MK-IK using the multiple kernel strategy in the trend branch can not provide better performance compared with TFDNet-IK on datasets with low channel-wise correlations. Considering that TFDNet-IK is dedicated to forecasting time

Table 11: Investigation of Trend-TFB. TFDNet-MK-IK means using TFB with multiples kernels in TrendEncoder of TFDNet-IK, and TFDNet-2MK means using TFB with multiple kernels in both SeasonalEncoder and TrendEncoder

Datasets		Traffic				Electricity				ETTm2			
Prediction Length T		96	192	336	720	96	192	336	720	96	192	336	720
TFDNet-IK	MSE	0.377	0.392	0.406	0.447	0.128	0.145	0.160	0.197	0.157	0.213	0.264	0.345
	MAE	0.256	0.263	0.266	0.287	0.221	0.237	0.253	0.285	0.244	0.282	0.318	0.371
TFDNet-MK-IK	MSE	0.373	0.388	0.404	0.445	0.128	0.146	0.160	0.195	0.157	0.216	0.267	0.347
	MAE	0.255	0.261	0.268	0.287	0.223	0.237	0.254	0.285	0.244	0.283	0.320	0.372
TFDNet-MK	MSE	0.354	0.372	0.388	0.428	0.129	0.147	0.163	0.200	0.158	0.214	0.264	0.347
	MAE	0.241	0.250	0.257	0.279	0.221	0.239	0.256	0.288	0.246	0.283	0.319	0.372
TFDNet-2MK	MSE	0.354	0.371	0.388	0.428	0.129	0.147	0.164	0.199	0.158	0.214	0.265	0.346
	MAE	0.242	0.250	0.257	0.277	0.221	0.238	0.257	0.287	0.247	0.284	0.320	0.372

series with low correlations across channels, Trend-TFB with a simple structure is more applicable in terms of performance and efficiency. TFDNet-2MK also does not provide better performance than TFDNet-MK. The results verify that Trend-TFB with a single shared kernel is sufficient for processing trend information.

E Algorithm

We present the details of algorithms designed in our paper. Algorithm 1 demonstrates the overall process of TFDNet. Algorithm 2 and Algorithm 3 respectively describe the detailed process of TrendEncoder and SeasonalEncoder.

Algorithm 1 TFDNet

- 1: **Input:** Input historical time series \mathbf{X} ; Input length L ; Predict length T ; Data dimension D ; STFT window S ; Stride l . Technically, we set S as $\{8, 16, 32\}$, l as $\{3, 8, 16\}$.
 - 2: $\mathbf{X} = \text{RevIN}(\mathbf{X})^\top$ $\mathbf{X} \in \mathbb{R}^{D \times L}$
 - 3: $\mathbf{X}_{tr} = \text{AvgPool}(\text{Padding}(\mathbf{X}))$ $\mathbf{X}_{tr} \in \mathbb{R}^{D \times L}$
 - 4: $\mathbf{X}_{se} = \mathbf{X} - \mathbf{X}_{tr}$ $\mathbf{X}_{se} \in \mathbb{R}^{D \times L}$
 - 5: $\mathbf{Z}_{se} = \text{Linear}(\text{SeasonEncoder}(\mathbf{X}_{se}, S_1), \dots, \text{SeasonEncoder}(\mathbf{X}_{se}, S_s))$ $\mathbf{Z}_{se} \in \mathbb{R}^{D \times L}$
 - 6: $\mathbf{Z}_{tr} = \text{Linear}(\text{TrendEncoder}(\mathbf{X}_{tr}, S_1), \dots, \text{TrendEncoder}(\mathbf{X}_{tr}, S_s))$ $\mathbf{Z}_{tr} \in \mathbb{R}^{D \times L}$
 - 7: $\mathbf{Z} = \mathbf{Z}_{se} + \mathbf{Z}_{tr}$ $\mathbf{Z} \in \mathbb{R}^{D \times L}$
 - 8: $\hat{\mathbf{X}} = \text{RevIN}(\text{Linear}(\mathbf{Z})^\top)$ $\hat{\mathbf{X}} \in \mathbb{R}^{T \times D}$
 - 9: **Return** $\hat{\mathbf{X}}$
-

Algorithm 2 TrendEncoder Procedure

- 1: **Input:** Input trend component \mathbf{X}_{tr} ; Input length L ; Data dimension D ; STFT window S_s ; Stride l_s .
 - 2: $\tilde{\mathbf{X}}_{tr} = \text{STFT}(\mathbf{X}_{tr}, S_s, l_s)$ $\tilde{\mathbf{X}}_{tr} \in \mathbb{C}^{D \times M \times N}$
 - 3: **For** i **in** $\{1, \dots, D\}$:
 - 4: $\mathbf{Q}_{tr}^{(i)} = \text{Kernel}(\tilde{\mathbf{X}}_{tr}^{(i)}, \mathbf{W}_{tr})$ $\mathbf{Q}_{tr}^{(i)} \in \mathbb{C}^{M \times N}, \mathbf{W}_{tr} \in \mathbb{C}^{M \times N \times N}$
 - 5: **End for**
 - 6: $\hat{\mathbf{Q}}_{tr} = \text{Linear}(\text{Reshape}(\mathbf{Q}_{tr}))$ $\hat{\mathbf{Q}}_{tr} \in \mathbb{C}^{D \times N \times M}$
 - 7: $\tilde{\mathbf{Z}}_{tr} = \mathbf{Q}_{tr} + \text{Reshape}(\text{Tanh}(\hat{\mathbf{Q}}_{tr}))$ $\tilde{\mathbf{Z}}_{tr} \in \mathbb{C}^{D \times M \times N}$
 - 8: $\mathbf{Z}_{tr} = \text{STFT}^{-1}(\tilde{\mathbf{Z}}_{tr}, S_s, l_s)$ $\mathbf{Z} \in \mathbb{R}^{D \times L}$
 - 9: **Return** \mathbf{Z}
-

Algorithm 3 SeasonalEncoder Procedure

1: **Input:** Input seasonal component \mathbf{X}_{se} ; Input length L ; Data dimension D ; STFT window S_s ; Stride l_s ; Hyper-parameter $mode$; Hyper-parameter I ; Hyper-parameter k .

2: $\tilde{\mathbf{X}}_{se} = \text{STFT}(\mathbf{X}_{se}, S_s, l_s)$ $\tilde{\mathbf{X}}_{se} \in \mathbb{C}^{D \times M \times N}$

3: **If** $mode == \text{IK}$:

4: $\mathbf{W}_{ind} = \mathbf{W}_1 \cdot \mathbf{W}_2$ $\mathbf{W}_{ind} \in \mathbb{C}^{D \times M \times N \times N}, \mathbf{W}_1 \in \mathbb{C}^{D \times I}, \mathbf{W}_2 \in \mathbb{C}^{I \times M \times N \times N}$

5: **For** i **in** $\{1, \dots, D\}$:

6: $\mathbf{Q}_{se}^{(i)} = \text{Kernel}(\tilde{\mathbf{X}}_{se}^{(i)}, \mathbf{W}_{ind}^{(i)})$ $\mathbf{Q}_{se}^{(i)} \in \mathbb{C}^{M \times N}$

7: **End for**

8: **End if**

9: **Else if** $mode == \text{MK}$:

10: **for** i **in** $\{1, \dots, D\}$:

11: **for** j **in** $\{1, \dots, k\}$:

12: $\mathbf{H}_j^{(i)} = \text{Kernel}(\tilde{\mathbf{X}}_{se}^{(i)}, \mathbf{W}_{multi}^j)$ $\mathbf{H}_j^{(i)} \in \mathbb{C}^{M \times N}, \mathbf{W}_{multi}^j \in \mathbb{C}^{M \times N \times N}$

13: $\mathbf{g}_j = \text{Sigmod}(|\sum \mathbf{G}^j \odot \tilde{\mathbf{X}}_{se}^{(i)}|)$ $\mathbf{G}^j \in \mathbb{C}^{M \times N}$

14: **End for**

15: $\mathbf{Q}_{se}^{(i)} = \sum_k \mathbf{g}_k \odot [\mathbf{H}_1^{(i)}; \mathbf{H}_2^{(i)}; \dots; \mathbf{H}_k^{(i)}]$ $\mathbf{Q}_{se}^{(i)} \in \mathbb{C}^{M \times N}$

16: **End for**

17: **End if**

18: $\hat{\mathbf{Q}}_{se} = \text{Linear}(\text{Reshape}(\mathbf{Q}_{se}))$ $\hat{\mathbf{Q}}_{se} \in \mathbb{C}^{D \times N \times M}$

19: $\tilde{\mathbf{Z}}_{se} = \mathbf{Q}_{se} + \text{Reshape}(\text{Tanh}(\hat{\mathbf{Q}}_{se}))$ $\tilde{\mathbf{Z}}_{se} \in \mathbb{C}^{D \times M \times N}$

20: $\mathbf{Z}_{se} = \text{STFT}^{-1}(\tilde{\mathbf{Z}}_{se}, S_s, l_s)$ $\mathbf{Z} \in \mathbb{R}^{D \times L}$

21: **Return** \mathbf{Z}
